Int. J. Heat Mass Transfer. Vol. 36, No. 3, pp. 809–822, 1993
Printed in Great Britain

0017-9310/93 $6.00 + 0.00

Analysis of heat and mass transfer during bulk hydraircooling of spherical food products

K. V. NARASIMHA RAO, G. S. V. L. NARASIMHAM and M. V. KRISHNA MURTHY
Department of Mechanical Engineering, Indian Institute of Science, Bangalore 560 012, India

(*Received* 30 *April* 1991)

Abstract—Hydraircooling is a technique used for precooling food products. In this technique chilled water is sprayed over the food products while cold unsaturated air is blown over them. Hydraircooling combines the advantages of both air- and hydrocooling. The present study is concerned with the analysis of bulk hydraircooling as it occurs in a package filled with several layers of spherical food products with chilled water sprayed from the top and cold unsaturated air blown from the bottom. A mathematical model is developed to describe the hydrodynamics and simultaneous heat and mass transfer occurring inside the package. The non-dimensional governing equations are solved using the finite difference numerical methods. The results are presented in the form of time–temperature charts. A correlation is obtained to calculate the process time in terms of the process parameters.

INTRODUCTION

HEAT AND mass transfer play a very important role in the food processing and preservation methods as discussed extensively in refs. [1, 2] on this subject. The aim of all food processing and preservation operations is to retard metabolic activity and growth of micro-organisms so that the product can be preserved for a longer time. Precooling is one such operation wherein the food products are cooled to their storage conditions by rapid removal of field and respiration heats immediately after harvest, gather or slaughter. Various types of precooling techniques like air cooling, hydrocooling and hydraircooling are discussed in detail in refs. [3, 4].

Hydraircooling is an efficient method of precooling food products for which moisture loss is not desirable. This concept combines the advantages of both air cooling and hydrocooling. When cold air is passed over the food products that are continuously wetted by a thin film of water, there will be more effective cooling without much moisture loss from the product compared to other conventional precooling methods [5]. This paper presents the results of a theoretical analysis of the bulk hydraircooling of spherical food products when the water and the air are flowing counter-current to each other. The governing equations for the product, film, interstitial water spray and the moist air are solved using finite difference methods. Time–temperature histories are obtained in terms of dimensionless parameters covering a wide range of the product properties and processing conditions encountered in food precooling practice.

THEORETICAL ANALYSIS

Description of the physical model

The physical model considers a number of layers of spherical food products packed in the form of a rectangular parallelepiped (Fig. 1). The geometry of the food product is chosen to be spherical because a large variety of fruits and vegetables can be satisfactorily approximated by this shape. Chilled water is sprayed on to the products so as to produce a thin film of water over each product (Fig. 2). The air is blown from the bottom of the package in a counter-flow direction. The food products are packed in horizontal layers, one below the other in an in-line arrangement in the vertical direction. The water film, as it flows enveloping the food product, experiences a certain amount of evaporation (from water film surface into moist air) or condensation (from moist air onto the film surface), depending on the direction of driving potential for mass transfer. When the film approaches the bottom of the product, the water gravitates on to the next food product directly below. This gives rise to the formation of a water film on the succeeding product. Some of the chilled water, however, is not intercepted by the food products and falls through the interstitial space of the packing. It is necessary to leave a small air gap between the product layers for ease of loading and unloading in practical situations. If the radius of the product is denoted by R and the height of air gap by B, the overall height of the package, H, containing L layers will be $L \cdot 2R + (L-1)B$ as shown in Fig. 1. A spherical coordinate system is employed for the food product with the radius r measured from the centre of the product while a Cartesian coordinate system is used with z-direction measured from the bottom of the package for the interstitial water spray and the moist air. Thus $z = H$ corresponds to the top of the package where water enters.

Initially, all the food products in the package are assumed to be at a uniform temperature T_{po}. The package is then exposed at the top of the first layer to a chilled water spray at a temperature of T_{fe}, while

NOMENCLATURE

a thermal diffusivity [$m^2 s^{-1}$]
A area [m^2]
A_0, A_1, A_2 coefficients defined in equation (26)
B_0, B_1, B_2 coefficients defined in equation (48)
C_0, C_1, C_2 coefficients defined in equation (50)
C_p specific heat [kJ $kg^{-1} K^{-1}$]
d diameter [m]
D binary diffusion coefficient of water vapour in dry air [$m^2 s^{-1}$]
D_1–D_4 coefficients defined in equation (60)
Fo Fourier number [dimensionless]
Fr Froude number [dimensionless]
g acceleration due to gravity [$m^2 s^{-1}$]
h_v enthalpy of water vapour [kJ kg^{-1}]
Δh_v latent heat of vaporization [kJ kg^{-1}]
H height of the package [m]
Ja Jakob number [dimensionless]
L number of layers
$\dot{m}$ mass flow rate [kg s^{-1}]
Nu Nusselt number [dimensionless]
Pr Prandtl number [dimensionless]
q_{int} heat of respiration in the food product [W m^{-3}]
r radial coordinate
R radius of the spherical food product [m]
Re Reynolds number [dimensionless]
Sc Schmidt number [dimensionless]
Sh Sherwood number [dimensionless]
t time [s]
T temperature [°C]
v_θ tangential velocity in the film [m s^{-1}]
w average velocity [m s^{-1}]
W humidity ratio [kg per kg of dry air]
z coordinate along the height of the package.

Greek symbols
α_h heat transfer coefficient [W $m^{-2} K^{-1}$]
α_m mass transfer coefficient [kg $m^{-2} s^{-1}$]
δ film thickness [m]
θ angular coordinate
λ thermal conductivity [W $m^{-1} K^{-1}$]
μ dynamic viscosity [N s m^{-2}]
ν kinematic viscosity [$m^2 s^{-1}$]
ρ density [kg m^{-3}]
$\tau_{0.2}$ process time [dimensionless]
ψ void fraction [dimensionless].

Subscripts
e entry
f water film
fbm fluid bulk mean
fi interstitial water spray
o initial
ma moist air
p product
s saturated (also used for superficial velocity)
u per unit volume of the package [m^{-3}]
wb wet bulb
wd water droplet.

Superscripts
*, ** dimensionless quantity.

cold unsaturated air at a temperature of T_{mac} is blown from the bottom of the package. The products are cooled by the combined action of chilled water and air. The conditions of entering water and air are maintained constant throughout.

Mathematical formulation

The bulk hydraircooling problem described above involves transient, simultaneous heat and mass transfer. The following assumptions are made to simplify the formulation:

(a) The food product is homogeneous and isotropic.
(b) The thermophysical properties of the product are independent of temperature [6].
(c) Moisture concentration gradients and internal moisture evaporation within the product are ignored [7].
(d) The product temperature is invariant in the azimuthal direction.
(e) Air temperature and humidity ratio vary only in the z-direction.
(f) Radiation heat transfer between the products is negligible because of the low ranges of temperatures encountered in precooling practice.

Governing equations

The governing equations are written separately for the product, water film over the product, the interstitial water spray and the moist air.

Product. The two-dimensional, transient conduction equation as applicable for the product in spherical coordinates is

$$\frac{\partial^2 T_p}{\partial r^2} + \frac{2}{r}\frac{\partial T_p}{\partial r} + \frac{\cot\theta}{r^2}\frac{\partial T_p}{\partial \theta} + \frac{1}{r^2}\frac{\partial^2 T_p}{\partial \theta^2} + \frac{q_{int}}{\lambda_p} = \frac{1}{a_p}\frac{\partial T_p}{\partial t} \quad (1)$$

Liquid film. The coordinate system for the liquid film is shown in Fig. 2. In view of the thinness of the film ($\mu_f \rho_f \gg \mu_{ma}\rho_{ma}$), the transverse pressure gradient is neglected and since the impressed pressure is

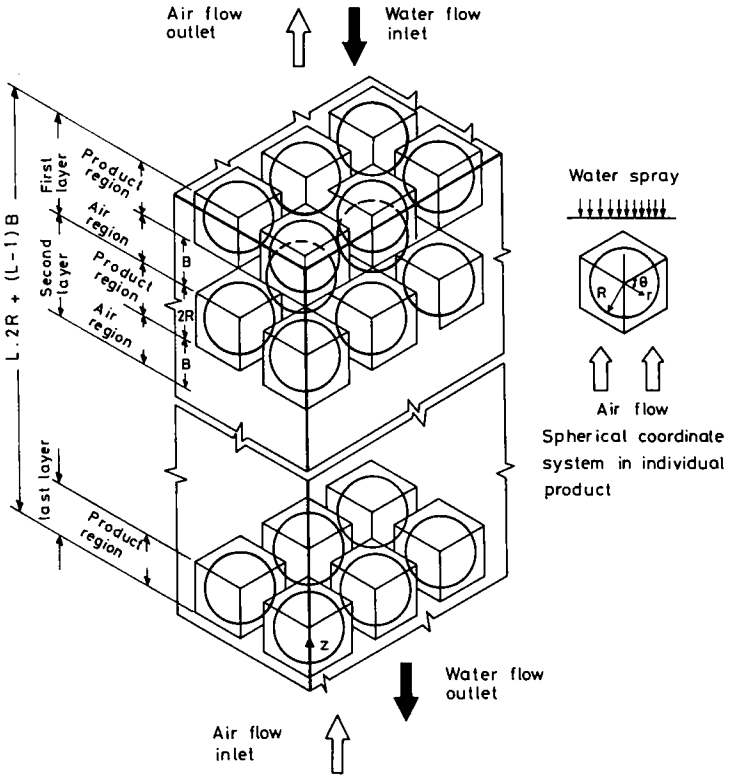

FIG. 1. The physical model and coordinate system for bulk hydraircooling of food products.

taken as constant, the streamwise pressure gradient becomes zero. The governing equation for the momentum in the liquid film with quasi-steady approximation is written as follows:

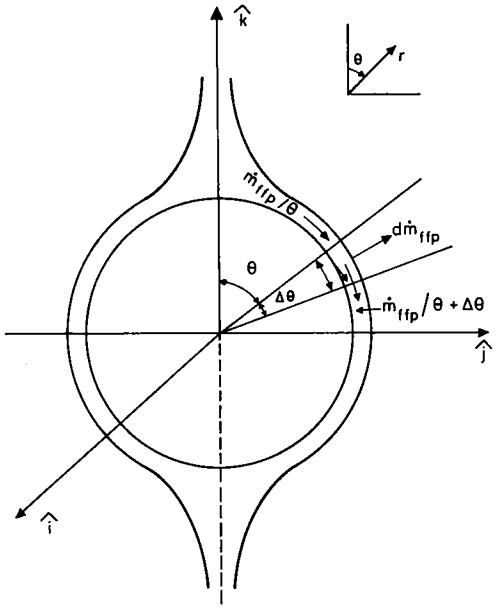

FIG. 2. Physical model.

Momentum equation

$$\mu_f \frac{d^2 v_\theta}{dr^2} + \rho_f g \sin\theta = 0. \quad (2)$$

The above equation is written under the assumption that the viscous forces balance the gravitational forces and hence the acceleration terms are negligible [8].

Energy equation

$$\frac{\partial T_f}{\partial t} + \frac{v_\theta}{R}\frac{\partial T_f}{\partial \theta} = a_f\left\{\frac{\partial^2 T_f}{\partial r^2} + \frac{1}{R^2}\frac{\partial^2 T_f}{\partial \theta^2}\right\}. \quad (3)$$

Mass conservation

$$\frac{d\dot{m}_{ffp}}{d\theta} = -\alpha_{mf} 2\pi R^2 \sin\theta (W_{sf} - W_{ma}). \quad (4)$$

Water spray.

Mass conservation

$$\frac{d\dot{m}_{fi}}{dz} = \alpha_{mwd} A_c A_{wdu} (W_{swd} - W_{ma}). \quad (5)$$

Here A_{wdu} is the area of water droplets available per unit volume of the package. The determination of this quantity requires the diameter of the water droplet and the number of water droplets contained in a unit volume of the package. In this investigation an average droplet diameter of 0.85 mm and an average droplet velocity of 10 m s^{-1} are used. The value of A_{wdu}

can then be calculated if the mass flow rate of water through the interstices is known. As will be seen later, these assumptions have, however, very little influence on the final results and the interstitial water spray is found to have a negligible effect on the bulk hydrair-cooling process.

Energy equation

$$\frac{\partial T_{wd}}{\partial t} = w_{wds}\frac{\partial T_{wd}}{\partial z} + \frac{w_{wds}}{m_{fi}} T_{wd}(\alpha_{mwd} A_c A_{wdu}(W_{swd} - W_{ma})) - \frac{w_{wds}}{\dot{m}_{fi} c_{pf}}(\alpha_{mwd} A_c A_{wdu}(W_{swd} - W_{ma})h_v + \alpha_{hwd} A_c A_{wdu}(T_{swd} - T_{ma})). \quad (6)$$

Moist air.

Energy equation

The equation for the conservation of energy in the moist air is written as follows:

$$\rho_{ma} C_{pma}\left(\psi\frac{\partial T_{ma}}{\partial t} + w_s\frac{\partial T_{ma}}{\partial z}\right) = \psi\lambda_{ma}\frac{\partial^2 T_{ma}}{\partial z^2} + \alpha_{hf} A_{fu}(T_{sf} - T_{ma}) + \alpha_{hwd} A_{wdu}(T_{swd} - T_{ma}) \quad (7)$$

where ψ is the void fraction which is defined as the ratio of the volume of the void to the total volume of any layer. ψ assumes a value of 1.0 in the air–water spray region as there are no products.

Conservation of species. The equation for the conservation of water vapor in the moist air can be written as follows:

$$\rho_{ma}\left(\psi\frac{\partial W_{ma}}{\partial t} + w_s\frac{\partial W_{ma}}{\partial z}\right) = \psi\rho_{ma} D\frac{\partial^2 W_{ma}}{\partial z^2} + \alpha_{mf} A_{fu}(W_{sf} - W_{ma}) + \alpha_{mwd} A_{wdu}(W_{swd} - W_{ma}). \quad (8)$$

Initial and boundary conditions

Product and film. The initial uniform temperature of the product gives the following condition:

$$\text{at } t \leqslant 0 \text{ for } 0 \leqslant r \leqslant R \text{ and } 0 \leqslant \theta \leqslant \pi, \quad T_p = T_{po}. \quad (9)$$

Symmetry of the temperature profile about the vertical axis yields:

$$\text{at } t > 0 \text{ for } 0 < r < R \text{ and at } \theta = 0 \text{ and } \pi, \quad \frac{\partial T_p}{\partial \theta} = 0. \quad (10)$$

An energy balance at the product–film interface results in:

$$\text{at } r = R \text{ for } 0 < \theta < \pi, \quad -\lambda_p\frac{\partial T_p}{\partial r} = -\lambda_f\frac{\partial T_f}{\partial r} \quad (11)$$

$$\text{also at } r = R \text{ for } 0 < \theta < \pi, \quad T_p = T_f = T_{if} \quad \text{(no temperature jump condition)} \quad (12)$$

where T_{if} is the product–film interface temperature.

$$\text{At } r = R, \quad v_\theta = 0, \quad \text{and} \quad (13)$$

$$\text{at } r = R+\delta, \quad \frac{dv_\theta}{dr} = 0. \quad (14)$$

The assumption of initially uniform temperature of the water film results in:

$$\text{at } t \leqslant 0, \text{ for } R \leqslant r \leqslant R+\delta \text{ and } 0 \leqslant \theta \leqslant \pi, \quad T_f = T_{f0}. \quad (15)$$

A continuous supply of spray water at T_{fe} is assumed to be available for the top layer to maintain a film of flowing water. This gives the condition:

$$\text{at } t > 0 \text{ for } R < r < R+\delta \text{ and at } \theta = 0, \quad T_f = T_{fe} \text{ (first layer)} \quad \text{or} \quad T_{fbm} \text{ (subsequent layers).} \quad (16)$$

Here T_{fbm} represents the bulk mean temperature of the fluid collected at the bottom of the preceding food product. The following expression is used to calculate the bulk mean temperature at any θ-coordinate:

$$\dot{m}_{ffp}|_\theta C_{pf} T_{fbm}|_\theta = \int_0^\delta \rho_f v_\theta 2\pi r \sin\theta C_{pf} T_f \, dr \quad (17)$$

$$\text{at } \theta = \pi \text{ and for } R < r < R+\delta, \quad \frac{\partial T_f}{\partial \theta} = 0. \quad (18)$$

At the surface of the liquid film which is in contact with the air, the energy transfer takes place due to the combined effect of heat and mass transfer. The temperature difference between the film surface and the free stream air acts as the driving force for the sensible heat transfer, whereas the vapor pressure difference causes evaporation of water at the film surface resulting in the transfer of latent heat. This boundary condition is written in terms of the sensible and latent heat transfers as follows:

$$\text{at } t > 0 \text{ and } r = R+\delta, \text{ for } 0 \leqslant \theta \leqslant \pi, \quad -\lambda_f\frac{\partial T_f}{\partial r} = \alpha_{hf}(T_{sf} - T_{ma}) + \alpha_{mf}(W_{sf} - W_{ma})\Delta h_v. \quad (19)$$

Water spray

$$\text{At } z = H, \quad \dot{m}_{fi} = \dot{m}_{fic} = \dot{m}_{fe} - \dot{m}_{ffe}. \quad (20)$$

$$\text{At } t = 0 \text{ for } 0 \leqslant z \leqslant H, \quad T_{wd} = T_{fo}. \quad (21)$$

$$\text{At } t > 0 \text{ at } z = H, \quad T_{wd} = T_{fe}. \quad (22)$$

Moist air

$$\text{At } t = 0 \text{ for } 0 \leqslant z \leqslant H, \quad T_{ma} = T_{mao} \quad \text{and} \quad W_{ma} = W_{mao}. \quad (23)$$

At $t > 0$ at $z = 0$, $T_{ma} = T_{mac}$ and $W_{ma} = W_{mac}$. (24)

$$\text{At } z = H, \quad \frac{\partial T_{ma}}{\partial z} = 0, \quad \text{and} \quad \frac{\partial W_{ma}}{\partial z} = 0, \quad (25)$$

The humidity ratio of saturated air is expressed as a second degree polynomial in terms of its temperature as follows:

$$W_s = A_0 + A_1 T_s + A_2 T_s^2 \quad (26)$$

where the coefficients A_0, A_1, and A_2 are constants shown below for a temperature range of 0–25°C

$$A_0 = 3.879 \times 10^{-3}$$
$$A_1 = 2.173 \times 10^{-4}$$
$$A_2 = 1.605 \times 10^{-5}. \quad (27)$$

The wet bulb temperature of the air at any point is found using the following psychrometric relation [9]

$$W_{ma} = \frac{(2501 - 2.381 T_{wb}) W_s - (T_{ma} - T_{wb})}{2501 + 1.805 T_{ma} - 4.186 T_{wb}}. \quad (28)$$

Non-dimensionalization

To obtain the solution in a generalized form so that it is applicable to a wide variety of products and processing conditions, the following non-dimensionalized variables are defined:

$$T^* = \frac{T - T_{wbe}}{T_{po} - T_{wbe}}; \quad r^* = r/R; \quad z^* = z/R;$$
$$H^* = H/R; \quad y_f^* = y_f/R, \text{ where } y_f = r - R;$$
$$\delta^* = \delta/R; \quad Fo = a_p t/R^2; \quad \lambda^* = \lambda_p/\lambda_f;$$
$$\lambda^{**} = \lambda_{ma}/\lambda_f; \quad a^* = a_p/a_f; \quad a^{**} = a_{ma}/a_f;$$
$$\nu^{**} = \nu_{ma}/\nu_f; \quad \rho^{**} = \rho_{ma}/\rho_f; \quad C_p^{**} = C_{pma}/C_{pf};$$
$$d_{wd}^* = d_{wd}/R; \quad v_\theta^* = v_\theta/(\dot{m}_{ffpe}/\rho_f R^2);$$
$$Re_f = \dot{m}_{ffpe}/\rho_f \nu_f R; \quad A_c^* = A_c/R^2;$$
$$Fr_f = [(\dot{m}_{ffpe}/\rho_f R^2)/\sqrt{(gR)}]; \quad A_{fu}^* = A_{fu} R;$$
$$A_{wdu}^* = A_{wdu} R; \quad Nu_f = \alpha_{hf} 2R/\lambda_{ma};$$
$$Sh_f = \alpha_{mf} 2R/\rho_{ma} D; \quad Re_p = w_s 2R/\nu_{ma};$$
$$Re_{wd} = w_{wds} d_{wd}/\nu_{ma}; \quad Re_{mwd} = (w_s + w_{wds}) d_{wd}/\nu_{ma};$$
$$Sc_{ma} = \nu/D; \quad Nu_{wd} = \alpha_{hwd} d_{wd}/\lambda_{ma};$$
$$Sh_{wd} = \alpha_{mwd} d_{wd}/\rho_{ma} D; \quad \dot{m}_{fi}^* = \dot{m}_{fi}/\dot{m}_{fe};$$
$$\dot{m}_{ffe}^* = \dot{m}_{ffe}/\dot{m}_{fe}; \quad \dot{m}_{fie}^* = \dot{m}_{fie}/\dot{m}_{fe};$$
$$Pr_f = \nu_f/a_f; \quad Pr_{ma} = \nu_{ma}/a_{ma}; \quad R_m = \dot{m}_{ffpe}/\dot{m}_{fe};$$
$$\dot{m}_{ma}^* = \dot{m}_{ma}/\dot{m}_{fe}; \quad Ja = C_{pf} \Delta T/\Delta h_v,$$
$$\Delta T = T_{po} - T_{wbe}; \quad q_{int}^* = [q_{int} R^2/\lambda_p \Delta T];$$
$$R_T = T_{wbe}/\Delta T. \quad (29)$$

The governing equations are now rephrased in terms of the above non-dimensional variables.

Dimensionless governing equations

Product.

$$\frac{\partial T_p^*}{\partial Fo} = \frac{\partial^2 T_p^*}{\partial r^{*2}} + \frac{2}{r^*}\frac{\partial T_p^*}{\partial r^*} + \frac{\cot\theta}{r^{*2}}\frac{\partial T_p^*}{\partial \theta} + \frac{1}{r^{*2}}\frac{\partial T_p^{*2}}{\partial \theta^2} + q_{int}^*. \quad (30)$$

Liquid film.

Momentum equation

$$\frac{d^2 v_\theta^*}{dy_f^{*2}} = -\frac{Re_f}{Fr_f^2}\sin\theta. \quad (31)$$

Energy equation

$$\frac{\partial T_f^*}{\partial Fo} + \frac{v_\theta^* Re_f Pr_f}{a^*}\frac{\partial T_f^*}{\partial \theta} = \frac{1}{a^*}\left[\frac{1}{\delta^{*2}}\frac{\partial^2 T_f^*}{\partial y_f^{*2}} + \frac{\partial^2 T_f^*}{\partial \theta^2}\right]. \quad (32)$$

Mass conservation

$$\frac{d\dot{m}_{ffp}^*}{d\theta} = -\frac{Sh_f}{2Re_f Sc_{ma}} \nu^{**}\rho^{**} 2\pi \sin\theta (W_{sf} - W_{ma}). \quad (33)$$

Water spray.

Mass conservation equation

$$\frac{d\dot{m}_{fi}^*}{dz^*} = \frac{Sh_{wd}\,\rho^{**}\nu^{**} A_{wdu}^* A_c^* R_m}{Re_f Sc_{ma} d_{wd}^*}(W_{swd} - W_{ma}). \quad (34)$$

Energy equation

$$\frac{\partial T_{wd}^*}{\partial Fo} = \frac{Re_{wd}\,\nu^{**} Pr_f}{a^* d_{wd}^*}\frac{\partial T_{wd}^*}{\partial z^*} + \frac{Re_{wd}\,Sh_{wd}\,\rho^{**}\nu^{**2} A_{wdu}^* A_c^* Pr_f R_m}{Re_f Sc_{ma} d_{wd}^{*2} a^* \dot{m}_{fi}^*} \times (T_{wd}^* + R_T)(W_{swd} - W_{ma}) - \frac{Re_{wd}\,Nu_{wd}\,\lambda^{**}\nu^{**} A_{wdu}^* A_c^* R_m}{Re_f d_{wd}^{*2} a^* \dot{m}_{fi}^*}(T_{swd}^* - T_{ma}^*) - \frac{Re_{wd}\,Sh_{wd}\,\rho^{**}\nu^{**2} A_{wdu}^* A_c^* Pr_f R_m (1 + Ja)}{Ja\,Re_f Sc_{ma} d_{wd}^{*2} a^* \dot{m}_{fi}^*} \times (W_{swd} - W_{ma}). \quad (35)$$

Moist air.

Energy equation

$$\psi\frac{\partial T_{ma}^*}{\partial Fo} + \frac{\dot{m}_{ma}^* Re_f Pr_f}{\rho^{**} A_c^* a^* R_m}\frac{\partial T_{ma}^*}{\partial z^*} = \psi\frac{a^{**}}{a^*}\frac{\partial^2 T_{ma}^*}{\partial z^{*2}} + \frac{Nu_f a^{**} A_{fu}^*}{2a^*}(T_{sf}^* - T_{ma}^*) + \frac{Nu_{wd}\,a^{**} A_{wdu}^*}{d_{wd}^* a^*}(T_{swd}^* - T_{ma}^*). \quad (36)$$

Conservation of species

$$\psi\frac{\partial W_{ma}}{\partial Fo}+\frac{m^*_{ma}\,Re_f\,Pr_f}{\rho^{**}A^*_c a^* R_m}\frac{\partial W_{ma}}{\partial z^*}$$
$$=\frac{Pr_f\,v^{**}}{Sc_{ma}\,a^*}\psi\frac{\partial^2 W_{ma}}{\partial z^{*2}}+\frac{Sh_f\,Pr_f\,A^*_{fu}v^{**}}{2Sc_{ma}\,a^*}(W_{sf}-W_{ma})$$
$$+\frac{Sh_{wd}\,Pr_f\,A^*_{wdu}v^{**}}{Sc_{ma}\,a^*d^*_{wd}}(W_{swd}-W_{ma}). \quad (37)$$

Initial and boundary conditions

$$Fo\leqslant 0,\text{ for }0\leqslant r^*\leqslant 1.0\text{ and }0\leqslant\theta\leqslant\pi,\quad T^*_p=1.0 \quad (38)$$

$$Fo>0,\text{ at }\theta=0\text{ and }\pi\text{ for }0<r^*<1.0,\quad \frac{\partial T^*_p}{\partial\theta}=0. \quad (39)$$

At $r^*=1.0$, for $0<\theta<\pi$,

$$\lambda^*\left.\frac{\partial T^*_p}{\partial r^*}\right|_{r^*=1}=\left.\frac{\partial T^*_f}{\partial y^*_f}\right|_{y^*_f=0}. \quad (40)$$

Also at $r^*=1.0$, for $0<\theta<\pi$, $T^*_p=T^*_f=T^*_{if}$. (41)

$$\text{At } y^*_f=0,\quad v^*_\theta=0,\quad\text{and} \quad (42)$$

$$\text{at } y^*_f=\delta^*,\quad \frac{dv^*_\theta}{dy^*_f}=0 \quad (43)$$

$$Fo\leqslant 0,\text{ for }0\leqslant y^*_f\leqslant\delta^*\text{ and }0\leqslant\theta\leqslant\pi,\quad T^*_f=T^*_{fo} \quad (44)$$

$$Fo>0,\text{ at }\theta=0\text{ and }0<y^*_f<\delta^*,\quad T^*_f=T^*_{fc}\text{ or }T^*_{fbm}. \quad (45)$$

The expression for the bulk mean temperature of the film crossing any radial line, T^*_{fbm}, is as follows:

$$T^*_{fbm}=\left\{\frac{1}{\dot m^*_{ffp}}\int_0^1 2\pi v^*_\theta\sin\theta T^*_f(1+y^*_f)\,dy^*_f\right\}. \quad (46)$$

$$\text{At }\theta=\pi\text{ and }0\leqslant y^*_f\leqslant\delta^*,\quad \frac{\partial T^*_f}{\partial\theta}=0. \quad (47)$$

At $y^*_f=\delta^*$ and $0\leqslant\theta\leqslant\pi$, that is, at the film surface,

$$-\frac{\partial T^*_f}{\partial y^*_f}=B_0+B_1T^*_{sf}+B_2T^{*2}_{sf} \quad (48)$$

where B_0, B_1 and B_2 are defined as shown below

$$B_0=-\frac{Nu_f\,\lambda^{**}T^*_{ma}}{2}+\frac{Sh_f\,Pr_{ma}\,\lambda^{**}}{2Sc_{ma}\,C_p^{**}\,Ja}(C_0-W_{ma})$$
$$B_1=-\frac{Nu_f\,\lambda^{**}}{2}+\frac{Sh_f\,Pr_{ma}\,\lambda^{**}}{2Sc_{ma}\,C_p^{**}\,Ja}C_1$$
$$B_2=\frac{Sh_f\,Pr_{ma}\,\lambda^{**}}{2Sc_{ma}\,C_p^{**}\,Ja}C_2. \quad (49)$$

In the above boundary condition, C_0, C_1 and C_2 are the coefficients of a quadratic expression of saturated humidity ratio at the film surface in terms of its temperature and are as follows:

$$W_{sf}=C_0+C_1T^*_{sf}+C_2T^{*2}_{sf} \quad (50)$$

where

$$C_0=A_0+A_1R_T\Delta T+A_2R_T^2\Delta T^2$$
$$C_1=A_1\Delta T+2A_2R_T\Delta T^2$$
$$C_2=A_2\Delta T^2. \quad (51)$$

$$\text{At } z^*=H^*,\quad \dot m^*_{fi}=\dot m^*_{ffc}=\dot m^*_{fc}-\dot m^*_{ffe} \quad (52)$$

$$Fo\leqslant 0,\text{ for }0\leqslant z^*\leqslant H^*,\quad T^*_{wd}=T^*_{fc} \quad (53)$$

$$Fo>0,\text{ at }z^*=H^*,\quad T^*_{wd}=T^*_{fc} \quad (54)$$

$$Fo\leqslant 0,\text{ for }0\leqslant z^*\leqslant H^*,\quad T^*_{ma}=T^*_{mae}\text{ and }W_{ma}=W_{mae} \quad (55)$$

$$Fo>0,\text{ at }z^*=0,\quad T^*_{ma}=T^*_{mae}\text{ and }W_{ma}=W_{mae}\text{ and} \quad (56)$$

$$\text{at } z^*=H^*,\quad \frac{\partial T^*_{ma}}{\partial z^*}=0\text{ and }\frac{\partial W_{ma}}{\partial z^*}=0. \quad (57)$$

The Nusselt number and the Sherwood number in equation (49) are evaluated using the following equations [10] which are valid for $Re_p>180$:

$$Nu_f=1.27(1-\psi)^{0.41}Re_p^{0.59}Pr_{ma}^{0.33}$$
$$Sh_f=1.27(1-\psi)^{0.41}Re_p^{0.59}Sc_{ma}^{0.33}. \quad (58)$$

The following correlations are used to determine the Nusselt number and the Sherwood number at the water droplet surface [11]:

$$Nu_{wd}=2.0+0.6Re_{mwd}^{0.5}Pr_{ma}^{0.33}$$
$$Sh_{wd}=2.0+0.6Re_{mwd}^{0.5}Sc_{ma}^{0.33}. \quad (59)$$

After finding the air dry bulb temperature T^*_{ma} and the humidity ratio, W_{ma}, the wet bulb temperature is determined using the following psychrometric relation:

$$D_1T^{*3}_{wb}+D_2T^{*2}_{wb}+D_3T^*_{wb}=D_4 \quad (60)$$

where

$$D_1=2.381C_2\Delta T$$
$$D_2=2.381C_1\Delta T+2.381C_2R_T\Delta T-2501C_2$$
$$D_3=2.381C_0\Delta T+2.381C_1R_T\Delta T-2501C_1-\Delta T-4.186\Delta TW_{ma}$$
$$D_4=2501C_0-2.381C_0R_T\Delta T-T^*_{ma}\Delta T-2501W_{ma}+2.381R_T\Delta TW_{ma}-1.805T^*_{ma}\Delta TW_{ma}. \quad (61)$$

METHOD OF SOLUTION

The following expressions for the film thickness (δ^*), and the tangential velocity (v_θ) are obtained by solving the film momentum equation:

$$\delta^*=\left(\frac{3Fr_f^2\,\dot m^*_{ffp}}{2\pi\sin^2\theta Re_f}\right)^{1/3} \quad (62)$$

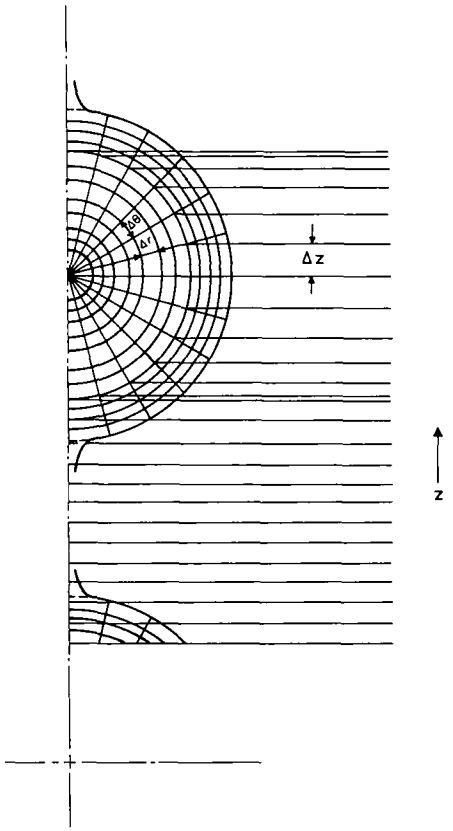

FIG. 3. Finite difference grid system for the product, film, and the accompanying air, water-spray region.

$$v_{fl}^* = \frac{Re_f}{Fr_f^2} \sin\theta\delta^* \left(\frac{y_f^*}{\delta^*} - \frac{1}{2}\frac{y_f^{*2}}{\delta^{*2}} \right). \quad (63)$$

The dimensionless governing equations along with the initial and boundary conditions are solved using finite difference techniques. The energy conservation equations for both the product and the film are solved simultaneously using the Peaceman–Rachford Alternating Direction Implicit (ADI) procedure. In view of the symmetry existing with respect to the vertical axis, only a semi-circular region of the product needs to be considered for numerical analysis. The computational domain and the layout of the finite difference grid are shown in detail in Fig. 3 for one product layer with the adjacent air gap. A non-uniform grid is adopted for the solution of moist air and water in the interstices between the products. This non-uniform grid is obtained by horizontally extending the radial lines ending on the product surface. In the region in between the product layers, a uniform grid is adopted.

Neither the temperature nor its radial gradient can be prescribed at the centre of the product owing to the non-existence of radial symmetry of the temperature profile about any radial line at the centre. This problem is overcome by employing a Cartesian coordinate system at the centre. After a number of numerical experiments, a grid size of (17×19) and a time step of 0.0025 are selected.

The finite difference analogues and the detailed method of solution are available in ref. [12].

All the computations are performed on the computer system VAX 8810 of the Indian Institute of Science, Bangalore. A typical run covering a dimensionless process time of 0.60 took about 250 s of CPU time. It may be noted that a dimensionless process time ($Fo = a_p t/R^2$) of 0.60 corresponds to 48 min of physical process time for an average value of $a_p = 1.3 \times 10^{-7}$ m^2 s^{-1} and for a typical product radius of 0.025 m.

Numerical solutions are obtained for the following values of the parameters so as to cover a wide range of precooling conditions of practical interest.

T_{fe}^* is varied from 0.0625 to 0.2187. This corresponds to the entering spray water temperature ranging from 5 to 10°C.

Re_f is varied from 5.0 to 50.0 in steps of 5.0. This corresponds to an entering water mass flow rate of 0.018–0.18 kg s^{-1}.

$\dot{m}_{ma}^*$ is varied from 0.5 to 10.0.

T_{mae}^* is varied from 0.0625 to 0.1875. This corresponds to an entering air dry bulb temperature of 5–9°C.

W_{mae} is varied from 0.0017 to 0.0046.

λ^* is varied from 0.1 to 1.0 in steps of 0.1. This corresponds to product thermal conductivity of 0.0585–0.585 W m^{-1} K^{-1} for a constant value of thermal conductivity of 0.585 W m^{-1} K^{-1} for water. These values cover a wide range of thermal conductivity values for common fruits and vegetables [9].

ψ is varied from 0.5 to 0.75 in steps of 0.025.

The values of the other parameters are as follows:

$$a^* = 0.9136; \quad a^{**} = 137.5; \quad A_c^* = 400.0;$$

$$C_p^{**} = 0.2402; \quad d_{wd}^* = 3.4 \times 10^{-2}; \quad Fr_f = 0.004;$$

$$Ja = 0.05; \quad L = 6; \quad Pr_f = 7.88; \quad Pr_{ma} = 0.7482;$$

$$q_{int}^* = 0.003; \quad Sc_{ma} = 0.665; \quad \lambda^{**} = 0.042;$$

$$\rho^{**} = 1.273 \times 10^{-3}.$$

It may be noted that the values of the dependent quantities A_{fu}^*, A_{wdu}^*, C_0, C_1, C_2, $\dot{m}_{ffe}^*$, $\dot{m}_{fie}^*$, Nu_f, Nu_{wd}, R_m, R_T, Re_p, Re_{mwd}, Sh_f, Sh_{wd}, and v^{**} can be calculated from those of other independent parameters.

Abdul Majeed [5] solved the hydraircooling problem for a single spherical product. In his analysis the water droplets and the air-side temperature and humidity distributions are not considered. The present analysis is used to reproduce his results for a typical set of parameters by considering a single product layer with a large void fraction ($\psi = 0.9948$). Satisfactory agreement is found between the two results as shown in Fig. 4, with the cooling times differing by about 4%. Thus single product hydraircooling problem can be thought of as a special case

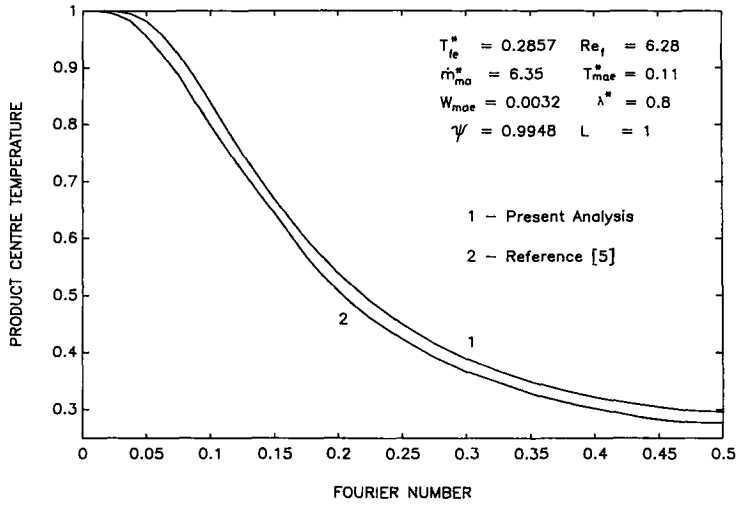

FIG. 4. Comparison of results for single product hydraircooling.

of the present, more general bulk hydraircooling problem.

RESULTS AND DISCUSSION

Typical time–temperature histories are presented in Fig. 5. It is observed that the cooling rate is slightly different for different layers. In general it is found that the first three layers from the top begin to cool faster initially. After a certain time, these layers lag behind the bottom layers. After a reasonably long time when a nearly steady state is reached, it can be seen that the bottom layers (layers 4, 5 and 6) have reached lower temperatures than the top layers, namely, layers 1, 2 and 3. This trend appears to be typical of a counter-current hydraircooling process and can be explained as follows.

The top layers cause a considerable rise in the temperature of water film initially. Also, the simultaneous heat and mass transfer occurring between the film and the air appears to be slightly insufficient to effect a considerable drop in the water film temperature and result in the same rate of cooling in the bottom layers. At larger times, the water film comes in contact with the already cooled product layers and the simultaneous heat and mass transfer from the water film to the air further reduces the temperature of the film as it flows down the package and results in a faster cooling in the bottom layers.

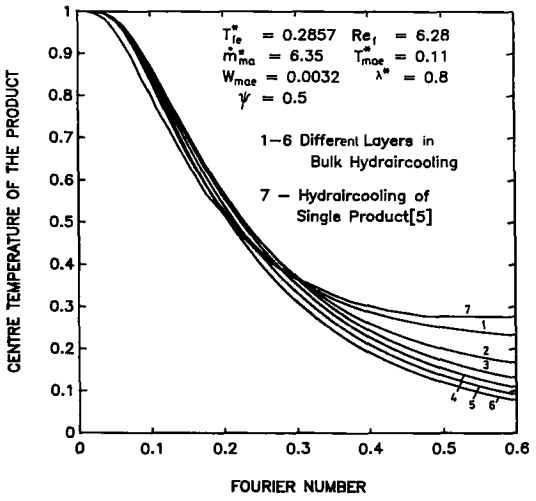

FIG. 5. Typical cooling curves during bulk hydraircooling and single-product hydraircooling.

The present model, though somewhat complex, is more realistic and predicts process times and final product temperatures which are substantially different from those predicted by a simple analysis for a single product. This can be clearly seen in Fig. 5 where the results of single-product hydraircooling of Abdul Majeed [5] are also presented for the same set of parameters. It can be seen from the latter part of the transient that lower final temperatures are possible in bulk hydraircooling as compared to the single-product hydraircooling. At a dimensionless time of 0.6, the product reaches a dimensionless temperature of about 0.275 during single product hydraircooling whereas the products reach much lower temperatures in the range of 0.08–0.17 (excepting the first layer) in bulk hydraircooling. For such final temperatures the single product analysis would predict the requirement of lower water and air inlet temperatures and/or higher velocities with the resulting increase in refrigeration capacity. It is also found in general that the bulk hydraircooling analysis predicts lower process times than the single product analysis. Thus the present, more general analysis leads to economical design and operation of the precooling equipment.

Figure 6 depicts a similar comparison with bulk air precooling process [13]. Both sets of curves are drawn for identical values of product and air parameters and for typical values of water conditions to facilitate a

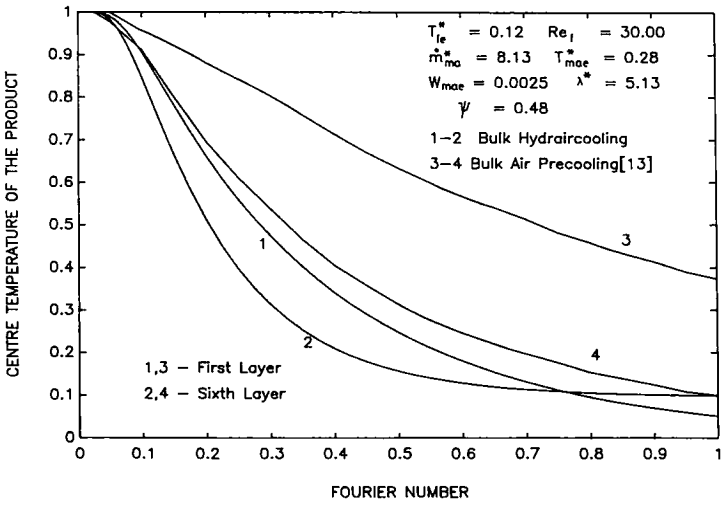

FIG. 6. Comparison of bulk hydraircooling with bulk air precooling.

realistic comparison. In each case the first and sixth layer in a six-layer package are considered for comparison. It is observed that bulk hydraircooling is much faster than the bulk air precooling. During conventional forced air precooling, only the product layers at the entry of the air are cooled faster than the farther layers with the process becoming ineffective beyond a certain number of layers. In bulk hydraircooling the air flowing through the package serves to abstract the combined sensible and latent heat from the water film thus maintaining the cooling potential of the film as it flows down the product layers. This permits the inlet water and air temperatures in bulk hydraircooling to be somewhat higher than those used in hydro- and air cooling practices. Thus the bulk hydraircooling process while resulting in lower final temperatures of the products and reduced processing times, also effects a saving in the energy required for refrigeration. Though the calculations presented here are performed for a six-layer package the process is found to remain effective for a much higher number of layers, the actual number of them being dependent upon the process conditions.

Figure 7 shows typical temperature profiles within the product and the film during bulk hydraircooling at different radial lines ($\theta = \pi/3$, $2\pi/3$) for different values of Fourier number. Temperatures are plotted from the product centre to film outer surface. The film thickness is plotted on a much enlarged scale. It can be seen that the product temperature decreases from the centre towards the surface of the product. With increasing time, it can also be seen that the temperature profile is becoming flatter. It is interesting to note that the film temperature variation is insignificant. This may be attributed to the thinness of the film.

The variation of the temperature in the product in the tangential direction at a time, $Fo = 0.2$, is shown in Fig. 8. It can be seen that the product temperature does not vary significantly in the tangential direction for the top layer. However, for the bottom layer, the temperature varies slightly, especially at the surface of the product. This could be due to the rapid rise in the temperature and humidity of the incoming air in the bottom-most layer.

Figure 9 shows the variation of temperature in the product at a fixed θ and at different radial distances with time, Fo. As is expected the product surface cools much faster than the interior.

Figure 10 shows the variation of product temperature with time at a fixed radial location and different angular positions. It can be seen that the temperature variation is insignificant with θ.

The interstitial water mass flow rate decreases by a very insignificant amount as it passes along the package. This is due to the evaporation of a small quantity of water from the water droplet surface into the air stream. Figure 11 shows the variation of interstitial water temperature as it passes along the package. Even a small quantity of water evaporating from the droplet surface causes considerable decrease in its temperature because of the large value of the enthalpy of evaporation associated with water. It can be seen that as time progresses the temperature variation becomes steeper.

Figure 12 shows the typical variation of air temperature as it passes through the package. Both the dry bulb and wet bulb temperatures are plotted on the same graph. It is observed that the air temperature varies almost linearly as it passes through the product layers and is more or less constant in the intervening space. This is due to the combined effect of the fortuitous property of a sphere—that its surface area varies linearly along any diametral axis, and the insignificant angular variation of the water film surface temperature. The air may pick up from or dissipate heat to two different sources: one is the film which has very large surface area and the other is water droplet which has a relatively smaller surface area. In

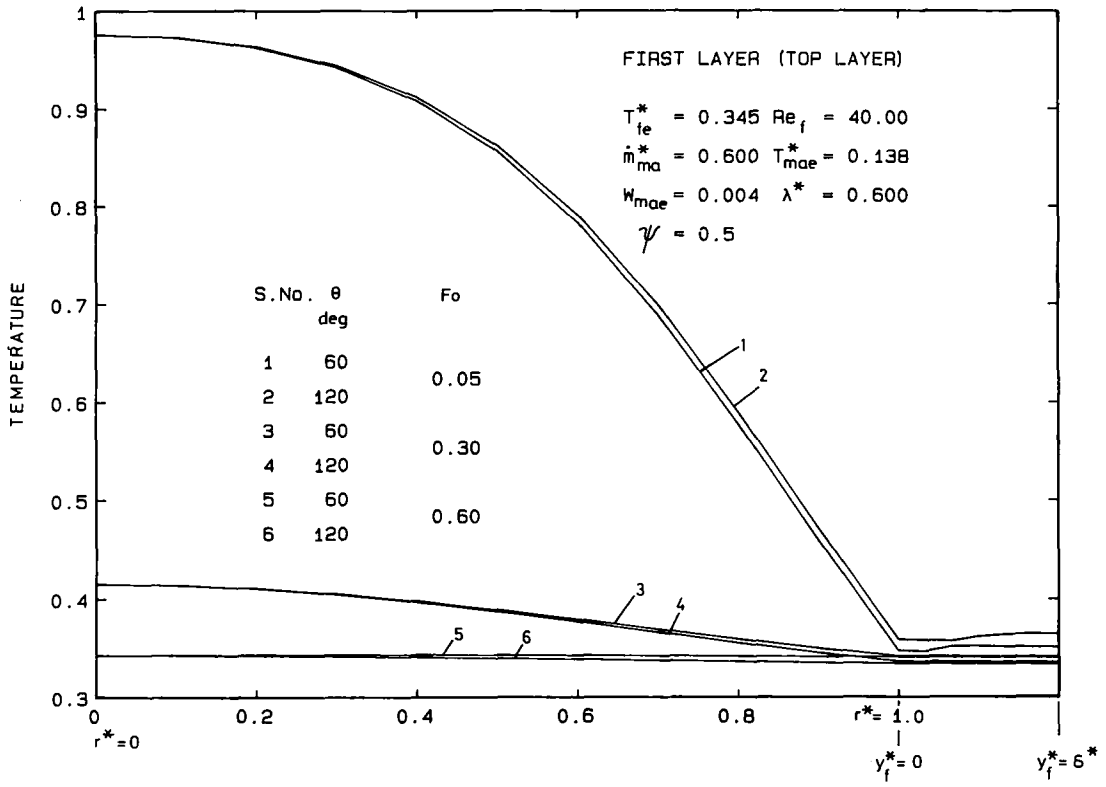

FIG. 7. Typical temperature profiles within the product and the film.

fact, the film surface area is two orders of magnitude higher than the water droplet surface area and hence the individual contribution from the surface of water droplets is very small.

The air may dissipate or pick up heat depending on the driving potential between air and the film surface at any location. Since the aim of hydraircooling process is to make use of the evaporation from the water film to the air stream as an additional cooling means, the parameters for the water and air like T_{fe}, T_{mae} and W_{mae} are so chosen in the present investigation that the air wet bulb temperature is always smaller than the water at any location for any time. These parameter values are estimated from a number of numerical experiments. The air thus picks up heat from the film surface as well as the water droplet surface and becomes hot. Because of the insignificant contribution from the water droplet surface area the air passes through the air layers without any noticeable change in its temperature.

Figure 13 shows the typical variation of air humidity ratio as it passes through the package. It is observed that the air is becoming more humid while passing through the package. The saturated humidity ratio corresponding to its temperature is also plotted in the same graph. Because of the large film surface area available for evaporation to take place, the entering air which is unsaturated picks up moisture, and the moisture pick up by air is higher in the product layers than in the air layers.

Figure 14 shows the time–temperature histories of actual food products (potatoes, peaches and apples) during bulk hydraircooling. The product dimensions, properties and the processing conditions are all depicted on the figure.

Process time

Process time is the time for which the hydraircooling is to be carried out to obtain the storage temperature suitable for the food product prior to transport. The storage temperature is different for different fruit and vegetables. For instance, for food products such as apples, cabbage, lettuce and peaches for which hydraircooling is desirable to avoid moisture loss, a storage temperature of about 10°C is required. This corresponds to a dimensionless temperature of about 0.2 for an initial product temperature of 35°C and entering air wet bulb temperature of .3°C. In the majority of the cases investigated, the top layer is found to take the maximum time to reach the storage temperature. Hence the time taken by the top layer to reach a dimensionless temperature of 0.2 is considered as the process time for the entire package.

Correlation for process time

A correlating equation for the process time $\tau_{0.2}$ in terms of the process parameters T^*_{fe}, Re_f, $\dot{m}^*_{ma}$, T^*_{mae},

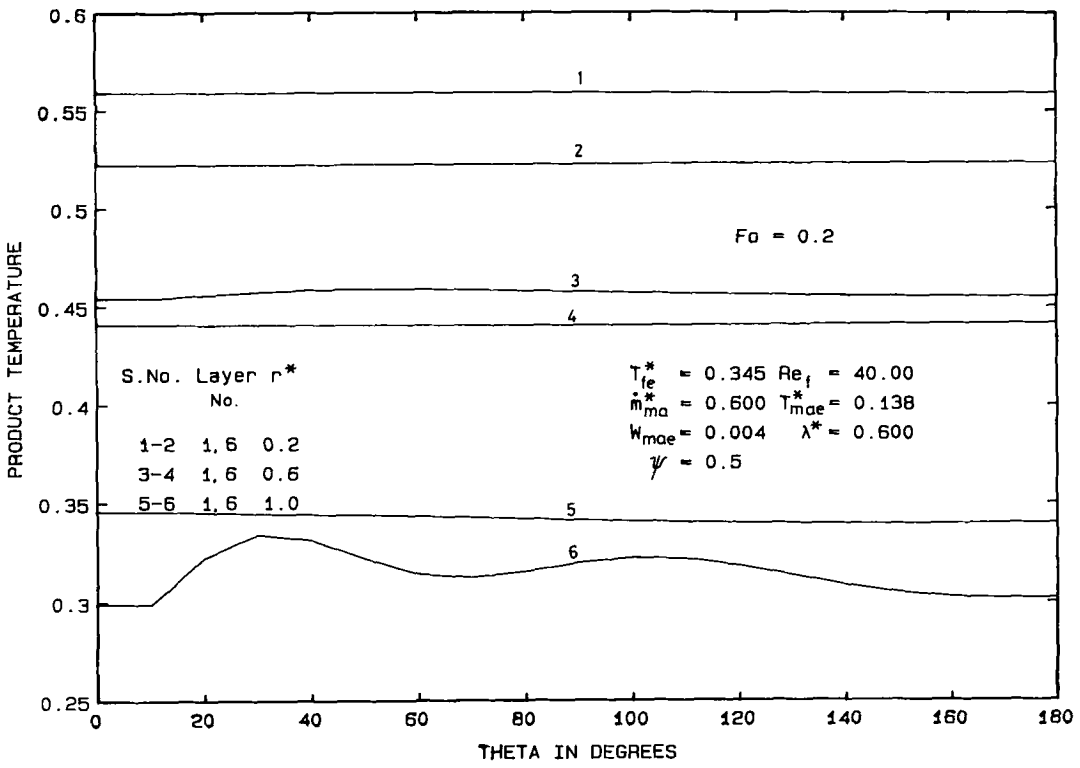

FIG. 8. Typical temperature profiles within the product.

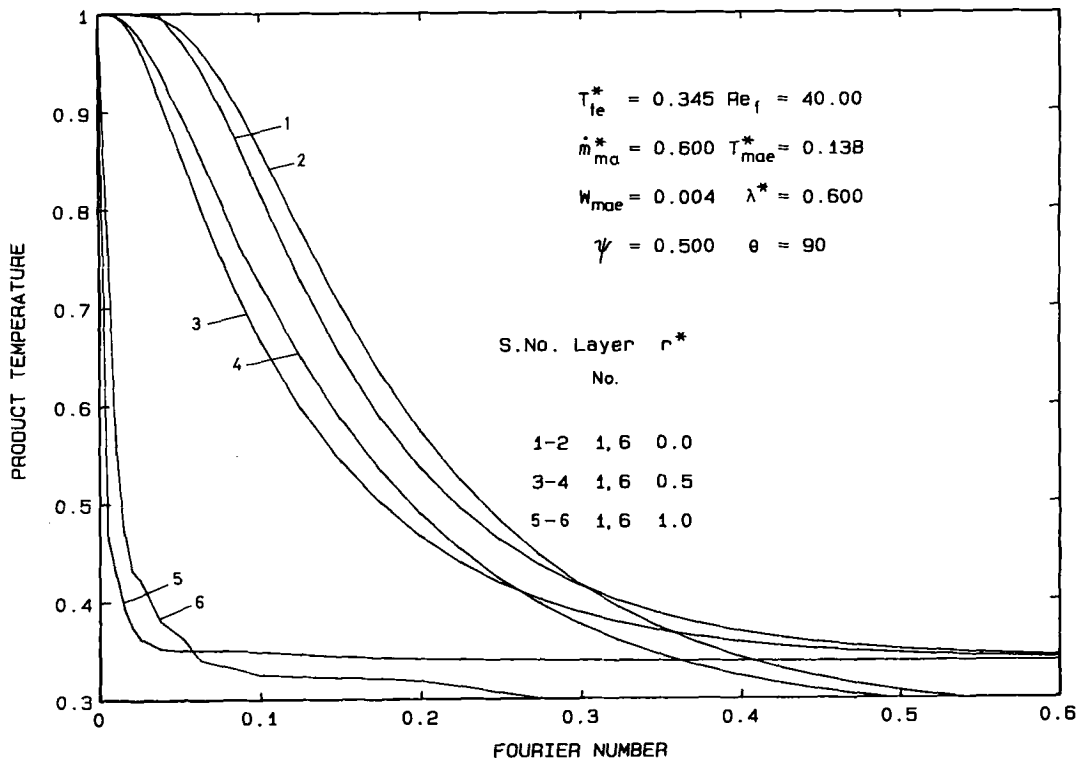

FIG. 9. Temperature variation in the radial direction.

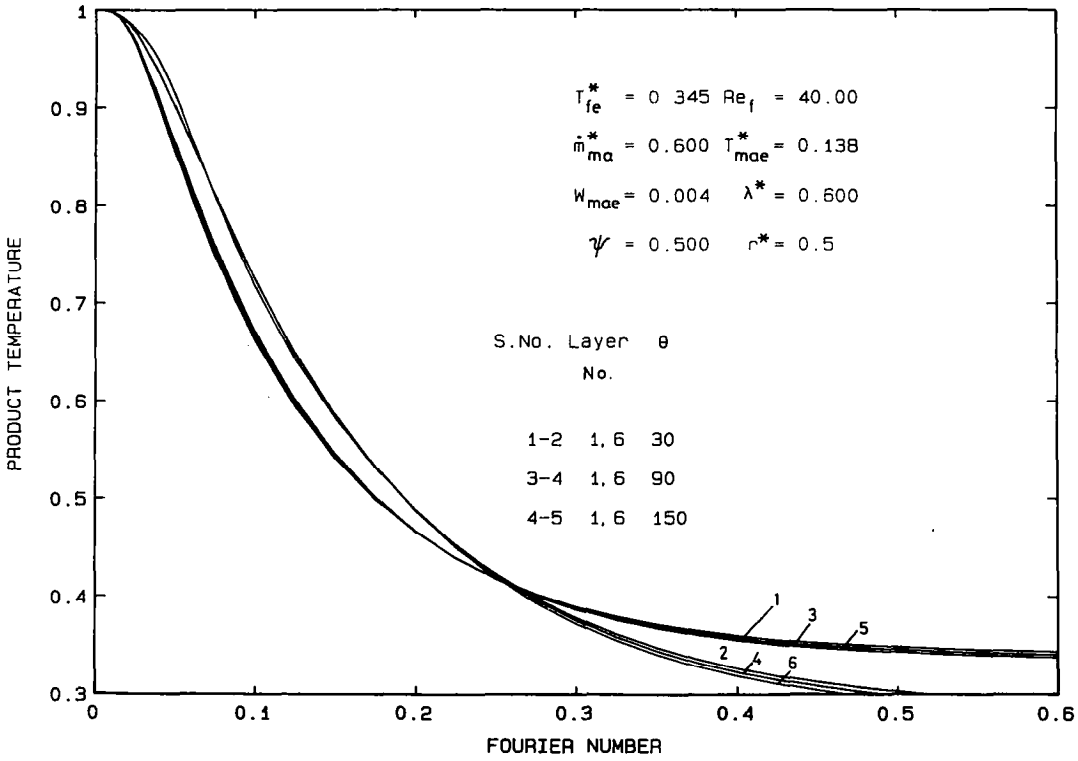

FIG. 10. Temperature variation in the tangential direction.

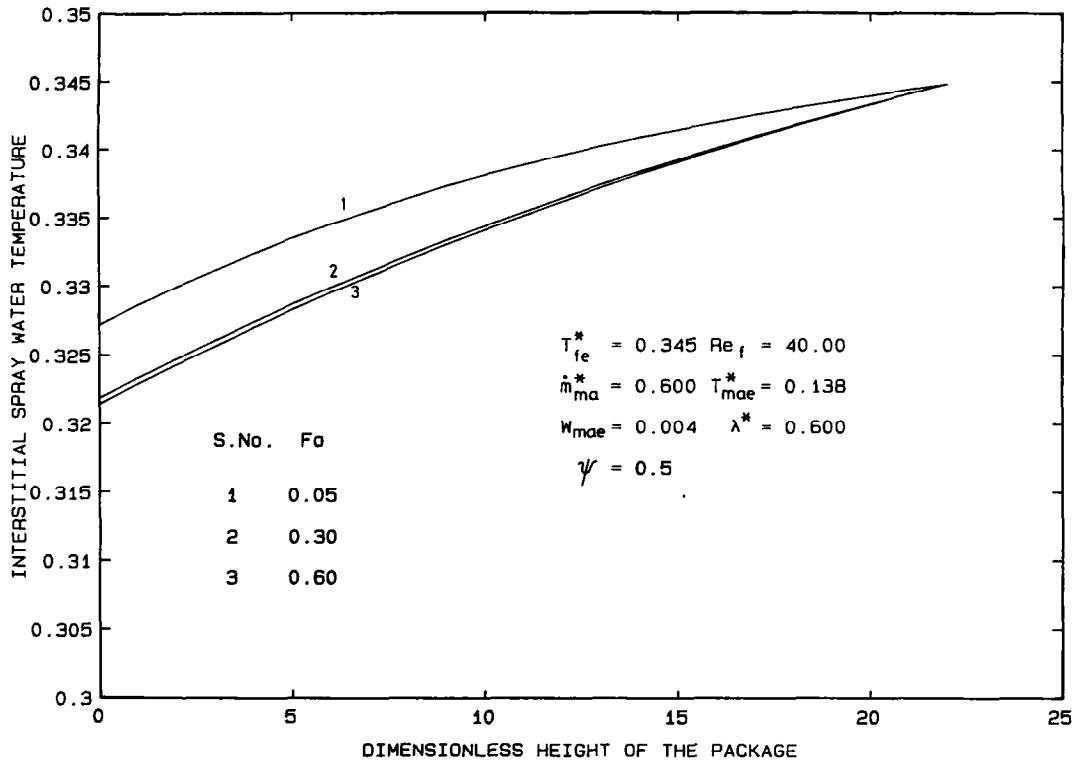

FIG. 11. Typical variation of spray water temperature.

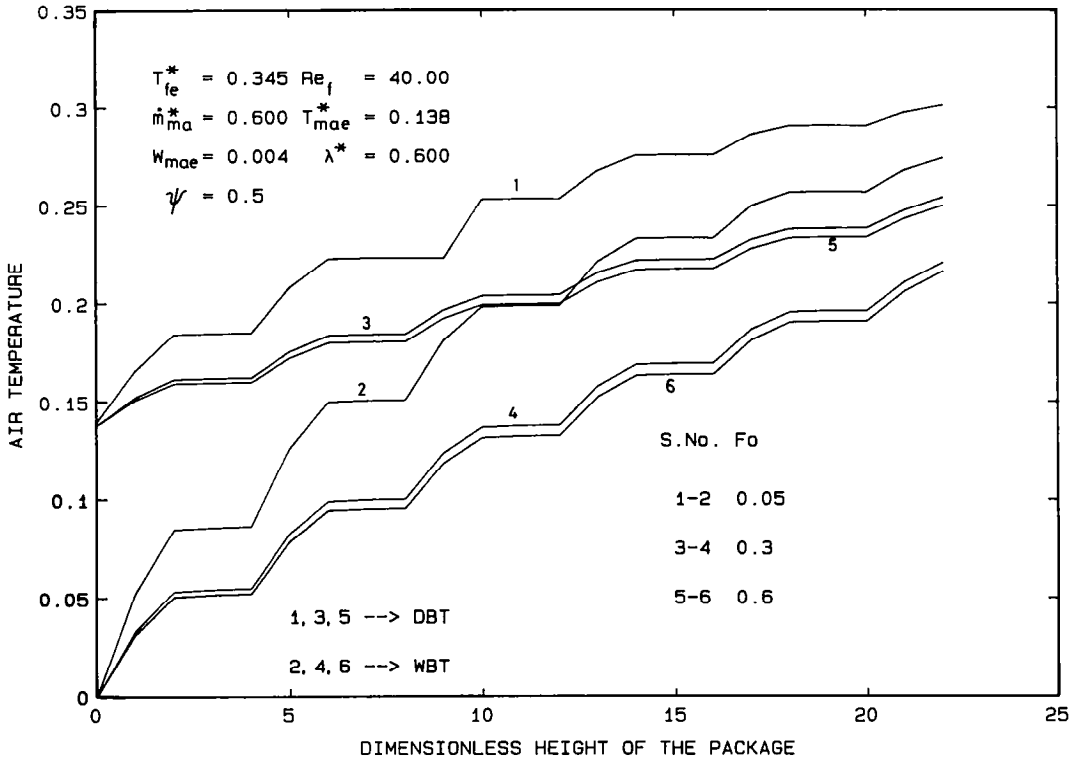

FIG. 12. Variation of air temperature.

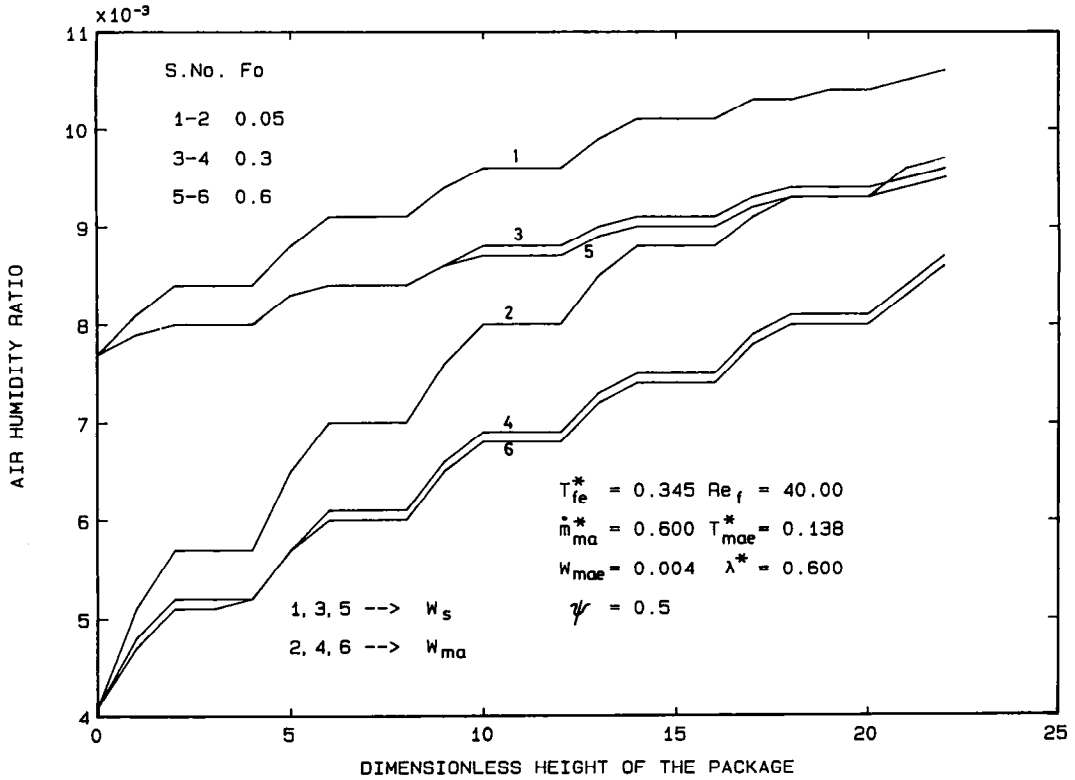

FIG. 13. Variation of air humdity ratio.

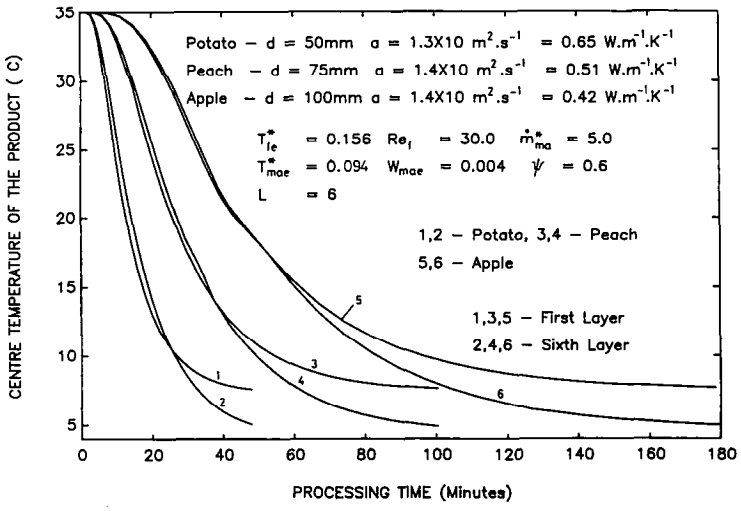

FIG. 14. Hydraircooling of actual food products.

W_{mae}, λ^*, and ψ is developed using multiple regression analysis. A total of 61 data points are used for correlating the process time. The correlation fits the data very well with the multiple correlation coefficient and the standard error of estimate being, respectively, 0.9364 and 0.021, and is given below

$$\tau_{0.2} = a0 T_{fe}^{*a1} Re_f^{a2} \dot{m}_{ma}^{*a3} T_{mae}^{*a4} W_{mae}^{a5} \lambda^{*a6} \psi^{a7} \quad (64)$$

where the value of the coefficient $a0$, and the exponents $a1$, $a2$, $a3$, $a4$, $a5$, $a6$ and $a7$ are: $a0 = 1.8428$; $a1 = 0.47$; $a2 = -0.0618$; $a3 = -0.0269$; $a4 = 0.0394$; $a5 = 0.0737$; $a6 = 0.0316$; $a7 = 0.0071$.

CONCLUSIONS

A mathematical model is developed to describe the simultaneous heat and mass transfer occurring during bulk hydraircooling of spherical food products. The governing equations are solved using finite difference numerical methods. The results are presented in the form of time–temperature charts. The present analysis yields final product temperatures which are substantially different from those obtained by a simple analysis for a single product. The effect of interstitial water spray on the cooling rate is found to be insignificant. A correlation is obtained for the process time in terms of the process parameters.

REFERENCES

1. M. V. Krishna Murthy and K. Badarinarayana, *Heat and Mass Transfer in Food Products, VI Int. Heat Transfer Conf.*, Toronto, Canada, 7–11 August, Vol. 6, pp. 339–353 (1978).
2. J. J. Gaffney, C. D. Baird and K. V. Chau, Methods for calculating heat and mass transfer in fruits and vegetables individually and in bulk, *ASHRAE Trans.* **91**(2B), 332–352 (1985).
3. *ASHRAE Guide and Data Book (Applications)*. American Society of Heating, Refrigerating and Air Conditioning Engineers, Inc., Atlanta, Georgia (1971).
4. E. G. Hall, Techniques of precooling, the long term storage, C. A. storage and the freezing of fruits and vegetables; Part I: precooling of fruit and vegetables, Int. Short Term Course, Durgapur, India, 14–24 January, F.A.O.–I.I.R., pp. 75–90 (1974).
5. P. M. Abdul Majeed, Analysis of heat transfer during hydraircooling of spherical food products, *Int. J. Heat Mass Transfer* **24**, 323–333 (1981).
6. I. Lamberg and B. Hallstrom, Thermal properties of potatoes and a computer simulation of a blanching process, *J. Fd Technol.* **21**, 577–585 (1986).
7. J. Soule, G. E. Yost and A. H. Bennett, Certain heat transfer characteristics of oranges, grape fruit and tangelos during forced-air precooling, *Trans. ASAE* **9**, 335–358 (1986).
8. M. C. Chyu and A. H. Bergles, An analytical and experimental study of falling-film evaporation on a horizontal tube, *Trans. ASME, J. Heat Transfer* **109**, 983–990 (1987).
9. *ASHRAE Hand Book, Fundamentals*. American Society of Heating, Refrigerating and Air Conditioning Engineers, Inc., Atlanta, Georgia (1989).
10. K. J. Beukema, S. Bruin and J. Schenk, Heat and mass transfer during cooling and storage of agricultural products, *Chem. Engng Sci.* **37**, 291–298 (1982).
11. R. B. Bird, W. E. Stewart and E. N. Lightfoot, *Transport Phenomena*. Wiley, New York (1960).
12. K. V. Narasimha Rao, Analysis of heat and mass transfer during bulk hydraircooling of food products, M.Sc.(Engng) thesis, Indian Institute of Science, Bangalore, India (1989).
13. K. Narasaiah Chetty, Heat and mass transfer during bulk precooling of food products, Ph.D. thesis, Indian Institute of Technology, Madras, India (1987).